Nigerian Journal of Technology (NIJOTECH)
Vol. 42, No. 1, March, 2023, pp.2 - 11
www.nijotech.com

Print ISSN: 0331-8443
Electronic ISSN: 2467-8821
https://doi.org/10.4314/njt.v42i1.2

EFFECTS OF HOMOGENOUS-HETEROGENEOUS REACTIONS ON STAGNATION POINT OF ALIGNED MHD CASSON NANOFLUID OVER A MELTING SURFACE

T. W. Akaje[1,*], B. I. Olajuwon[1] and M. T. Raji[1]

[1]Department of Mathematics, Federal University of Agriculture, Abeokuta, Ogun State, Nigeria

*corresponding author (Email: akajewasiu@gmail.com)

Article history: Received 27 March, 2022. Revised 07 February, 2023. Accepted 09 February, 2023

Abstract

This study examines how melting heat transfer affects the MHD Casson nanofluid's stagnation point when there are both homogeneous and heterogeneous chemical reactions occurring along with viscous dissipation. Additionally taken into account in this study are the effects of thermophoresis and Brownian motion. The linked non-linear partial differential equations that control nanofluid flow can be reduced to couple non-linear ordinary differential equations using local similarity variables, which can then be numerically solved using the Spectral Collocation technique, as demonstrated in the current flow mathematical modeling. Both qualitative and quantitative data are presented to show how flow control settings affect fluid flow, temperature, and nanoparticle concentration. The comparison of the current results with previously published works revealed good agreement, as shown in table 1.

Keywords: Casson nanofluid, Homogeneous-heterogeneous reactions, Inclined magnetic field, Melting heat transfer, Nonlinear thermal radiation.

1.0 INTRODUCTION

Since there is no direct relationship between stress and deformation rate, non-Newtonian fluids have been employed in a variety of sectors during the last decade, It has a wide range of applications, including biofluid dynamics, polymer production, petroleum drilling, and, to name a few. Fluids come in a variety of forms. Because of its multiple useful applications, the Casson fluids model is one of the most important non-Newtonian models. When shear stress is less than yield stress, Casson fluid acts like a solid, but when shear stress exceeds yield stress, it deforms. As a result, this fluid has a shear-thinning viscosity at zero rate shear yield stress, below which no flow occurs, and a viscosity of zero at infinite rate of shear. Several researchers have researched Casson fluid extensively.

For instance, [1] examined the impact of Newtonian heating on heat transmission in Casson fluid flow across an extended sheet with viscous dissipation. [2] investigated the steady incompressible fluid flow of a Casson nanomaterial generated by an angle "" with the vertical direction and determine that the values of Cfx (0) rise with weaker Nb, K and correlate to a decrement in this [3] investigated how chemical reactions affect MHD Casson fluid slip flow on a stretched sheet with heat and mass transfer. [4] examined the implication of thermal Marangoni convection in a dusty Casson fluid two-phase flow. The suspension of dust particles in the base fluid, according to their findings, boosted the heat transmission rate.

[5] studied the hall current effect on chemically reacting MHD Casson fluid flow with Dufour effect and thermal radiation and discovered that the skin-friction coefficient decreases as the magnetic parameter, Schmidt number, Prandtl number, chemical reaction parameter, and temperature increase. [6] study Casson fluid's unstable mobility on a wavy surface in the presence of a magnetic field. They discovered that the existence of viscosity in the fluid decreases velocity, as does the presence of partial slip velocity at the surface, and that increasing radiation enhances heat and mass transfer while

lowering skin friction. Copious studies on the Casson fluid model are [7-10].

Melting is often assumed to be the outcome of a physical change in the body as a result of the healing process. It changes a material from a solid to a liquid state. The melting problem has long been a subject of theoretical and experimental investigation. This is owing to its near proximity to a wide range of technologically vital processes. Researchers have made significant progress in the field of melting heat transfer as a result of its a broad range of scientific and industrial applications, including the production of semiconductor substances, the thawing of frozen soils, and the solidification of molten rock flows, to name a few. [11] examined the melting heat transfer of a hyperbolic tangent fluid across a stretched sheet and discovered that raising the melting parameter increases the velocity boundary layer thickness while lowering the thermal boundary layer thickness. [12] investigated the melting heat and mass transport features of an incompressible generalized Burgers fluid over a stretched sheet with a non-linear radiative heat flow. As the melting parameter was increased, the velocity profile got flatter, while the temperature distribution became flatter. According to [13], the fluid temperature and the thermal boundary layer thickness decrease for increasing thermal radiation and melting parameter whereas reverse effect occurs for stretching parameter, permeability parameter, and magnetic field parameter.

[14] study how melting and medium permeability affect the hydromagnetic wedge flow in a Casson nanofluid. By transitioning from the tube-and-shell model to the combine-and-shell model. [15] investigate enhanced melting heat transfer in latent thermal energy storage.

The majority of spontaneous chemical reactions are homogeneous and heterogeneous in nature. Many reactions proceed very slowly in the absence of a catalyst. As a result, it is highly difficult to investigate the connections between homogeneous and heterogeneous reactions, particularly the synthesis and consumption of reactant species at different rates with the fluid and on the catalyst surface. [16] pioneered the investigation of isothermal homogeneous-heterogeneous reactions in viscous fluid boundary layer flow on a flat surface, and his findings reveal that homogeneous reactions prevail downstream. More study on homogeneous-heterogeneous reactions was conducted to expand Merkin's reaction model. [17] used a semi analytical approach to study the effect of homogeneous and heterogeneous chemical processes on Oldroyd-B fluid flow in the presence of velocity and thermal slip is investigated. The homogeneous chemical reaction parameter is thought to improve the concentration profile, whereas the heterogeneous chemical reaction parameter is thought to diminish it. [18] studied the numerical behaviour of an incompressible two-dimensional Prandtl fluid flow on a stretched sheet under the impact of homogeneous and heterogeneous chemical characteristics. [19] studied Sisko fluid flow in the vicinity of a stretched cylinder with a convective boundary condition and homogeneous and heterogeneous reactions.

When the curvature parameter was increased, the thickness of the momentum and heat boundary layers increased, but the concentration boundary layer's thickness fell. [20] examined numerical modeling for homogeneous heterogeneous reactions and Newtonian heating in a nonlinear stretched cylinder flow of silver-water nanofluid. They notice that raising the magnetic parameter lowers the velocity profile while increasing the temperature profile. [21] investigated the homogeneous–heterogeneous interactions in the Casson fluid stagnation point flow caused by a stretching/shrinking sheet with uniform suction and sliding effects. Many researchers reported homogeneous and heterogeneous chemical reaction investigations in fluid flow are included in [22-25]. According to the author's knowledge, no previous work on homogeneous and heterogeneous chemical reactions studies in the fluid flow of MHD Casson nanofluid in the presence of a magnetic field that is inclined has been done, and this scientific effort is a major advance over earlier investigations mentioned in the above homogeneous and heterogeneous reactions literature review.

2.0 MATHEMATICAL ANALYSIS

The conducting incompressible stagnation point of Casson viscous dissipative laminar fluid of two-dimensional flow through a stretchy device is examined in the presence of melting heating with linear sheet speed rate along the direction and where and are constants, the movable sheet velocity is given by the melting surface temperature is assumed to be T_m, and the ambient temperature is expected to be T_1, with $T_m > T_1$. Cm is the concentration at the sheet's surface, whereas C_1 represents the ambient concentration. The magnetic field is considered to be inclined to the flow direction with negligible magnetic field induction. By applying little strain, the conducting free resting stress fluid creates an impulsive stretchy plate, and the Casson induced fluid material structure is preserved from deformation. An induced working fluid including surfactant nanoparticles prevents nanoparticle agglomeration. Fluid Newtonian heating and material species mass transfer are considered while creating a viscoplastic nanofluid. Figure 1 depicts the flow, heat, and mass model as [1-2] using boundary layer approximations. [2] Defines the Casson incompressible fluid's isotropic rheological state equation:

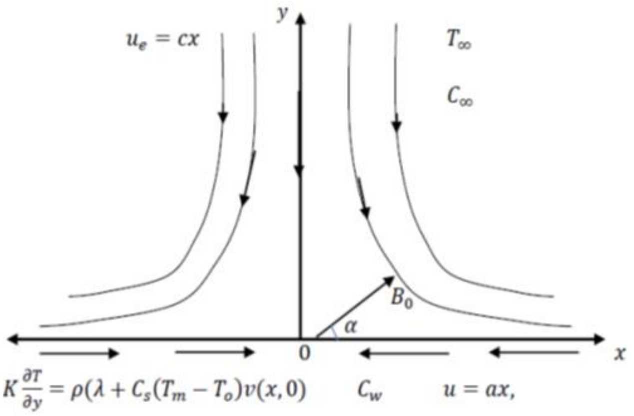

Figure 1: Schematic flow coordinate diagram

$$\tau_{ij} = \begin{cases} \left(\mu_B + \dfrac{P_y}{\sqrt{2\pi}}\right) 2e_{ij}, & \pi > \pi_c \\ \left(\mu_B + \dfrac{P_y}{\sqrt{2\pi_c}}\right) 2e_{ij}, & \pi < \pi_c \end{cases} \tag{1}$$

$$e_{ij} = \frac{1}{2}\left(\frac{\partial u_i}{\partial x_j} + \frac{\partial u_j}{\partial x_i}\right) \tag{2}$$

Where p_y denotes fluid yield stress, μ_B defines non-Newtonian dynamical fluid viscoplastic, π describes deformation product components with self, and $\pi = e_{ij}e_{ij}, e_{ij}$ in which $(i, j)^{th}$ represents deformation module and π_c is the non-Newtonian critical based value of π. Owing to the mentioned assumptions, the flow equation structures are presented as [5-7]: Furthermore, in a boundary layer flow, a simple model for the interaction of homogeneous and heterogeneous processes involving the two chemical species A and B is expressed by [1-2] is given below:

$$\begin{aligned} A + 2B \rightarrow 3B,\ rate = k_c ab^2 \\ A \rightarrow B,\ rate = k_s a \end{aligned} \tag{3}$$

Where a, b is the concentration of the chemical species A and B. The rates constant are k_c and k_s.

$$\frac{\partial u}{\partial x} + \frac{\partial v}{\partial y} = 0 \tag{4}$$

$$u\frac{\partial u}{\partial x} + v\frac{\partial u}{\partial y} = u_e\frac{du_e}{dx} + v\left(1 + \frac{1}{\beta}\right)\frac{\partial^2 u}{\partial y^2} + \frac{\sigma B_0^2(u_e - u)}{\rho} sin^2\alpha \tag{5}$$

$$u\frac{\partial T}{\partial x} + v\frac{\partial T}{\partial y} = \frac{k}{\rho c_p}\frac{\partial^2 T}{\partial y^2} + \tau\left[D_B\left(\frac{\partial C}{\partial y}\frac{\partial T}{\partial y}\right) + \frac{D_T}{T_\infty}\left(\frac{\partial T}{\partial y}\right)^2\right] + \frac{\mu}{\rho c_p}\left(1 + \frac{1}{\beta}\right)\left(\frac{\partial u}{\partial y}\right)^2 - \frac{1}{\rho c_p}\frac{\partial q_r}{\partial y} + \frac{\sigma B_0^2(u_e - u)}{\rho} sin^2\alpha \tag{6}$$

$$u\frac{\partial a}{\partial x} + v\frac{\partial a}{\partial y} = D_A\frac{\partial^2 a}{\partial y^2} - K_c ab^2 \tag{7}$$

$$u\frac{\partial b}{\partial x} + v\frac{\partial b}{\partial y} = D_B\frac{\partial^2 a}{\partial y^2} - K_c ab^2 \tag{8}$$

together with the given appropriate conditions:

$$u = ax, k\frac{\partial T}{\partial y} = \rho\big(\lambda + c_s(T_m - T_0)\big)v(x,0), D_A\frac{\partial a}{\partial y} = k_s C_1, D_B\frac{\partial b}{\partial y} = -k_s b\ at\ y = 0 \tag{9}$$

$$u \rightarrow u_e, T \rightarrow T_\infty, C_1 \rightarrow C_\infty, C_2 \rightarrow 0, as\ y \rightarrow \infty \tag{10}$$

From the stated models u and v depict the flow rate modules in (x, y)-axes, T and C are the nanofluid temperatures and the fractional nanoparticles volume correspondingly, $k\,is$ the fluid heat conductivity, σ stands for fluid electrical conductivity, v defines kinematic viscosity, $\alpha = \dfrac{k}{(\ell C_p)f}$ represents fluid heat diffusivity, $\tau = \dfrac{(\ell C_p)_p}{(\ell C_p)_f}$ describes the base fluid nanoparticles thermal capacity ratio, $D_B\ and\ D_T$ are the Brownian and thermophoretic distribution coefficients, ρ implies density of the fluid, T_∞ represents the temperature of far stream, T_w denotes sheet plate temperature, c_p depicts specific heat, and B_0 represents the strength of the inclined magnetic field, a thermal diffusivity, D the mass diffusivity, v the kinematic viscosity, $(T_o\ C_s)$ the temperature and heat capacity of the solid surface, λ the latent heat of the fluid, respectively.

Utilizing Rosseland's approximation q_r is defined as:

$$q_r = -\frac{4\sigma_s}{3k^*}\frac{\partial T^4}{\partial y} = -\frac{16\sigma_s}{3k^*}T^3\frac{\partial T}{\partial y} \tag{11}$$

In which σ and k^* are respectively the Stefan-Boltzman term and the coefficient absorption mean. Hence, Equaation (5) can be written in the form:

$$u\frac{\partial T}{\partial x}+v\frac{\partial T}{\partial y} = \frac{k}{\rho c_p}\frac{\partial^2 T}{\partial y^2}+\tau\left[D_B\left(\frac{\partial C}{\partial y}\frac{\partial T}{\partial y}\right)+\frac{D_T}{T_\infty}\left(\frac{\partial T}{\partial y}\right)^2\right] + \frac{\mu}{\rho c_p}\left(1+\frac{1}{\beta}\right)\left(\frac{\partial u}{\partial y}\right)^2\frac{16\sigma_s}{3k\rho c_p}\frac{\partial}{\partial y}\left(T^3\frac{\partial T}{\partial y}\right) + \frac{\sigma B_0^2(u_e-u)}{\rho c_p}sin^2\alpha \tag{12}$$

With the aid of the below transformations:

$$\eta=\left(\frac{u_w}{vx}\right)^{\frac{1}{2}}y, \psi(x,y)=(u_w v)^{1/2}\, xf(\eta), T = T_\infty\big(1+(TR-1)\theta(\eta)\big)\ \phi(\eta) = \frac{(C-C_\infty)}{(C_w-C_\infty)} \tag{13}$$

The function $\psi(x,y)$ represents stream function which is expressed as:

$$u=\frac{\partial\psi}{\partial y}, v=-\frac{\partial\psi}{\partial x}$$

The dimensionless model becomes,

$$\left(1+\frac{1}{\beta}\right)f'''+ff''-f'^2+A^2+Msin^2\alpha(A-f')=C \tag{14}$$

$$\frac{1}{Pr}(1+Rt(1+(TR-1)\theta)^3\theta')'+f\theta'+N_b\phi'\theta'+N_t\theta'^2+\left(1+\frac{1}{\beta}\right)Ecf''^2+EcM(A-f')^2sin^2\alpha=0 \tag{15}$$

$$\frac{1}{Sc}g''+fg'-Kgh^2=0 \tag{16}$$

$$\frac{\delta}{Sc}h''+fh'+Kgh^2=0 \tag{17}$$

$$\begin{cases} f'(0)=1, \theta(0)=0, Me\theta'(0)=-Prf(0), g'(0)=K_s g(0), -h'(0)=\frac{K_s}{\delta}g(0), \\ f'(\infty)=A, \theta(\infty)=1, g(\infty)=1, h(\infty)=0 \end{cases} \tag{18}$$

Furthermore, the diffusion coefficients of chemical species A and B are expected to be identical in size, leading us to infer that the diffusion coefficients D_B and D_A are equal. We assume, following [16], that the ratio of diffusion coefficients. Using the following assumptions, taking $\delta=1$, let's look at a relationship:

$$g(\eta)+h(\eta)=1 \tag{19}$$

Therefore, Equations (16) and (17) reduce to:

$$\frac{1}{Sc}g''+fg'-kg(1-g)^2=0 \tag{20}$$

The emerging terms in the above mathematical model are defined below as:

$$Pr=\frac{v}{\alpha}, S_c=\frac{v}{D_B}, M=\frac{\sigma B_o^2}{\rho b}, Ec=\frac{u_m^2}{c_p(T_m-T_\infty)}, N_R=\frac{16\sigma_s T_\infty^3}{3kk^*},$$
$$T_R=\frac{T_m}{T_\infty}, A=\frac{a}{c}, K_s=\frac{k_s Re^{-\frac{1}{2}}}{D_A}, N_b=\frac{(\rho c)_p D_B(C_m-C_\infty)}{\rho c_p v},$$
$$N_t=\frac{(\rho c)_p D_T(T_m-T_\infty)}{\rho c_p v T_\infty}, Re=\frac{c}{v}, \delta=\frac{D_B}{D_A}, K=\frac{k_c a_o}{c}, Me=\frac{C_f(T_m-T_o)}{\lambda+C_s(T_m-T_o)}$$

Pr is Prandtl number, M is a magnetic term, Ec is the Eckert number, N_t and N_b respectively denote the thermophoresis and Brownian motion terms, N_R denoted the thermal radiation parameter, T_R is the temperature ratio and A is the stretching ratio parameter, Sc is the Schmidt number, K is the measure of the strength of the homogeneous reaction, K_s is the measure of the strength of the heterogeneous reaction, and δ is the ratio of the coefficient of diffusion.

The local drag force C_{fx}, local temperature gradient Nu_x, and local mass gradient Sh_x are presented as follows:

$$C_{fx}=\frac{\tau_w}{\rho u_w^2}, Nu_x=\frac{xq_w}{k(T_w-T_\infty)}, Sh_x=\frac{xq_m}{D_B(C_w-C_\infty)},$$
$$\tau_w=\left(\mu_B+\frac{p_y}{\sqrt{2\pi_c}}\right)\left(\frac{\partial u}{\partial y}\right)_{y=0}, q_w=-k\left(\frac{\partial T}{\partial y}\right)_{y=0}+(q_r)_w, q_m = -D_B\left(\frac{\partial C}{\partial y}\right)_{y=0} \tag{21}$$

where shear stress is τ_w, the plate heat and mass flux q_w and q_m respectively. The dimensionless forms are:

$$Re_x^{1/2}C_f=\left(1+\frac{1}{\beta}\right)f''(0), \frac{Nu}{Re_x^{1/2}} = -\left(1+Rt\big((TR-1)\theta(0)+1\big)^3\right)\theta'(0), \frac{Sh_x}{Re_x^{1/2}} = -\emptyset'(0) \tag{22}$$

$Re_x=\frac{xu_w}{v}$ implies the Reynolds local number.

3.0 NUMERICAL TECHNIQUE

To find a computational solution for the current system, the Chebyshev spectra-collocation method is applied to solve the differential Equations. (14), (15) and (20) with the boundary condition (18). Among its numerous advantages over other methods is that it has high accuracy, efficiency and ability to solve both nonlinear and linear ODEs/ PDEs systems of equations. [26] described the Chebyshev nth-order polynomial defined by $T_n(\xi)$; $n\geq 0$ as :

$$T_n(\xi) = \cos(n \cos^{-1} \xi);\ -1 \le \eta \le 1 \tag{23}$$

The recursive formula is written as $T_{n+1} = 2xT_n(x) - T_{n-1}(x);\quad n \ge 1$.the range of the flow $[0, \infty)$ is approximately taken as [0, L] in other to introduce CSCM. The far domain of the boundary is L and the value of L defines the far stream convergence of the solution. Therefore, the range [0, L] is converted to the range [-1, 1] using the following algebraic definition:

$$\xi = \frac{2\eta}{L} - 1, \xi\ \epsilon[-1, +1] \tag{24}$$

Let assume that $f(\eta)$, $\theta(\eta)$ and $\phi(\eta)$ is the unknown basis function $T_k(\xi)$. to be approximated.

$$\left.\begin{aligned} f(\eta) &= \sum_{k=0}^{N} a_k T_k(\eta) \\ \theta(\eta) &= \sum_{k=0}^{N} b_k T_k(\eta) \\ \phi(\eta) &= \sum_{k=0}^{N} c_k T_k(\eta) \end{aligned}\right\} \tag{25}$$

where a_k, b_k *and* c_k are unknown coefficients to be obtained? Therefore, to have the residual equations, Eqn. (20) used on the governing equations (11)- (13), where the coefficient a_n, b_n and c_n are taken to reduce the residual error as low as possible between the considered range. Chebyshev collocation is used which is expressed according to Ehrenstein and Peyret [21].

$$\eta_j = \cos\left(\frac{\pi j}{N}\right), \qquad j = 0, ..., N. \tag{26}$$

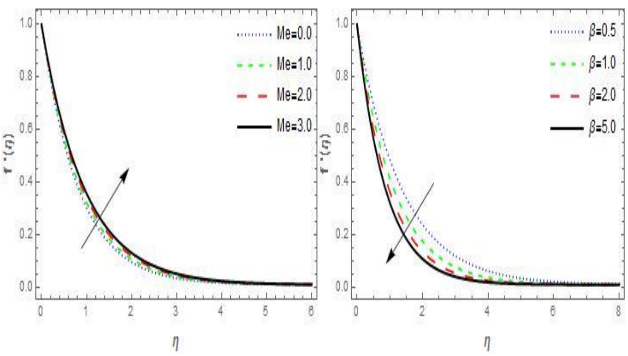

Figure 2: Concequence of Me and β on $f'(\eta)$

This produces a $3N+3$ set of algebraic equations along with the $3N+3$ coefficients a_k, b_k, and c_k to be determined. An iterative Newton's technique following from Finlayson [20] is employed on the resulting residues $N = 30$. Hence, the boundary value algorithm is established in Mathematica software to obtain the computational results for the problem.

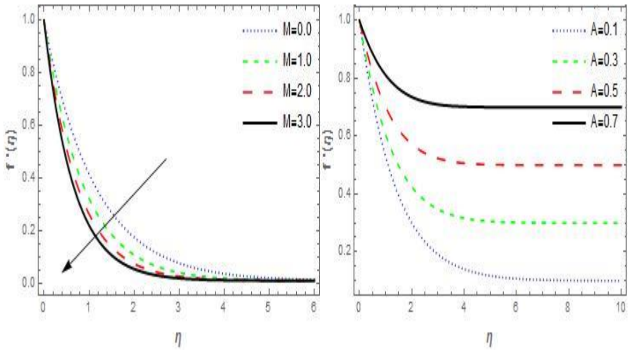

Figure 3: Concequence of M *and* A on $f'(\eta)$

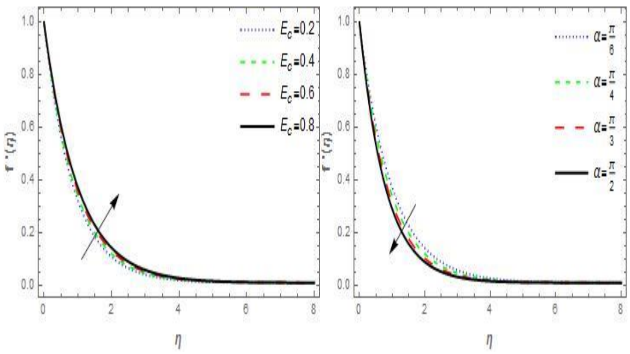

Figure 4: Concequence of E_c *and* α on $f'(\eta)$

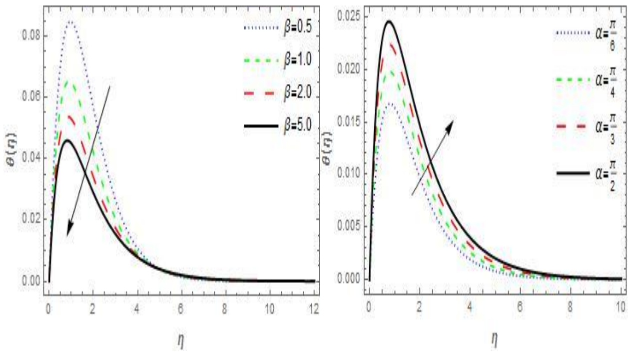

Figure 5: Concequence of β *and* α on $\theta(\eta)$

4.0 DISCUSSION OF RESULTS

For a variety of physical elements, a thorough numerical investigation is carried out, and the results are presented in graphs and tables. For various fluid parameter values, the governing equations were solved using the spectral collocation approach. The validity of the current technique was demonstrated by comparing our results to those of [27] and [28] for Nulset and Sherwood numbers for various values, which provided adequate precision for our current results. The values utilized in the current study are taken into account throughout the computation, unless otherwise specified in the framework. Figure 2 depicts the influence of melting heat (Me) and Casson parameters (β) on non-dimensional fluid flow. It is demonstrated that increasing the melting parameter (Me) decreases the velocity of the fluid and the thickness of the velocity boundary layer, whereas increasing the Casson term decreases the boundary viscosity film and velocity field; this observation is similar to that of [8].

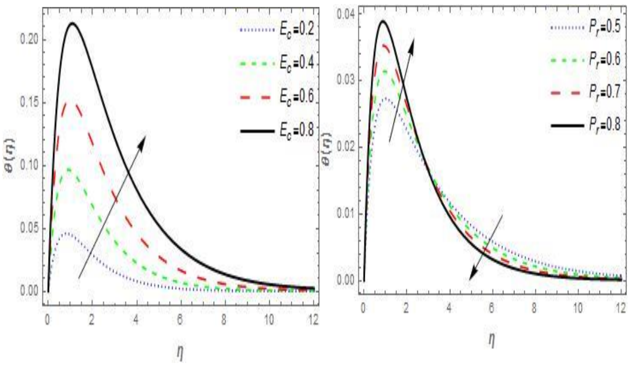

Figure 6: Concequence of E_c *and* P_r on $\theta(\eta)$

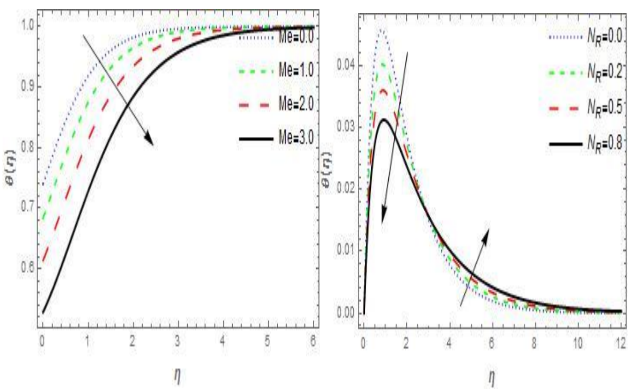

Figure 7: Concequence of Me *and* N_R on $\theta(\eta)$

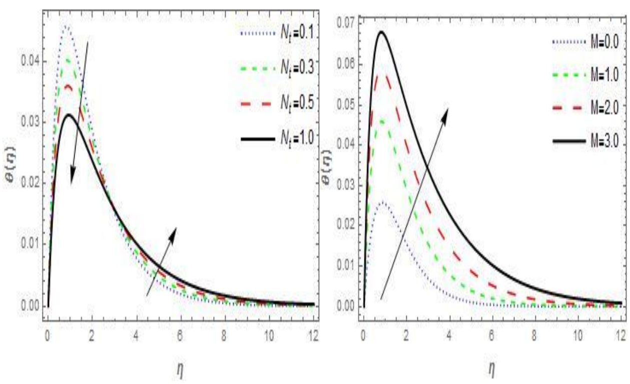

Figure 8: Concequence of Me *and* N_R on $\theta(\eta)$

The magnitude of flow speed for Casson liquids is greater than that of viscous liquids, as seen in Figure 2. Figure 3 depicts the interaction between the magnetic field and the velocity ratio. According to this graph, the inclined magnetic field slows the nano-Casson flow field and reduces the thickness of the boundary layer. As the inclined magnetic field grows, so does the resistance to fluid motion, which raises the incentive of the Lorentz force and the resistance to free flow movement. As the velocity ratio rises, both the flow velocity profile and the boundary viscosity layer expand. Figure 4 depicts the impact of and on dimensional velocity profiles. Increasing the value of figure 4 caused a drop in the velocity profile. This pattern is apparent when the aligned angle increases in value, which boosts the applied magnetic field and provides the opposing force to flow after raising the magnetic field, known as the Lorentz force, and as the aligned angle increases, resistance on the fluid particle increases. Meanwhile, increasing the number in figure 4 improves fluid flow.

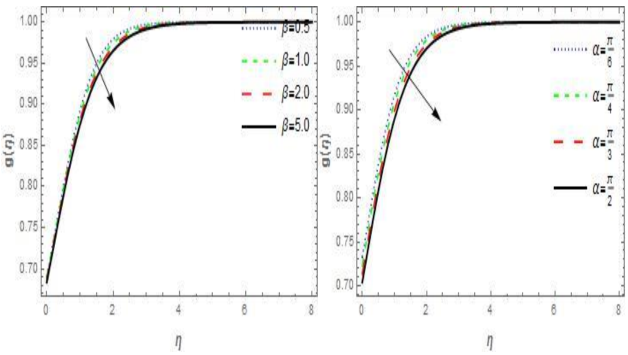

Figure 9: Concequence of β *and* α on $g(\eta)$

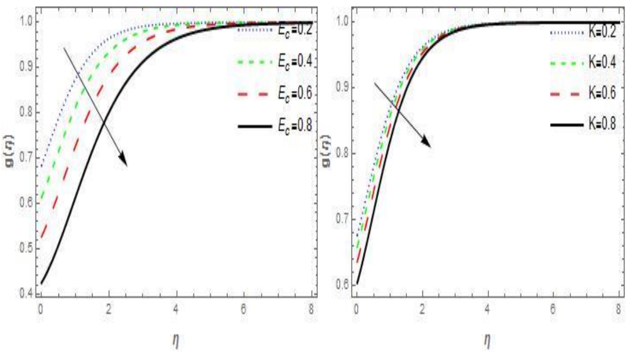

Figure 10: Concequence of E_c *and* K on $g(\eta)$

Figure 5 depicts the temperature solution profiles across the viscosity of the boundary layer for various dimensionless Casson parameter values. Raising the Casson parameter lowered the temperature profiles and thermal boundary layer, as shown in the graph. Figure 6 displays the impact of and numbers. As shown, raising the Eckert number enriches the temperature distribution, which correlates to heat dissipation and dispersion in a system. Because of the high particle impact and low fluid mass molecular bonding, heat propagation is preferred in this case. The heat field is also enhanced to increase heat conductivity and diffusion. Meanwhile, the temperature distribution improved as values near the stretching surface increased, but for a certain value of, the temperature will be equal for all indices, most likely at =3.0 after a while it decreases as it moves far away due to huge values of a term that leads to a reduction in fluid heat conductivity, which also decreases fluid temperature.

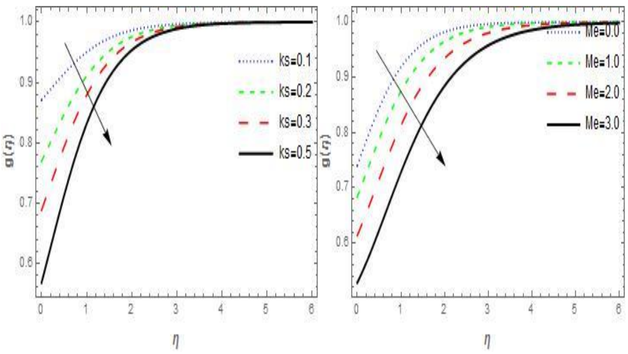

Figure 11: Concequence of k_s *and* Me on $g(\eta)$

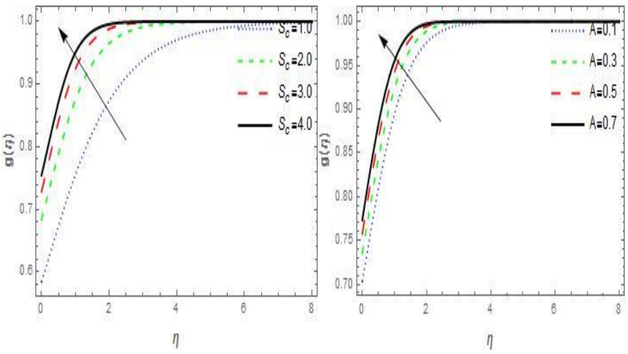

Figure 12: Concequence of S_c *and* A on $g(\eta)$

Figure 7 displays the effects of the melting parameter and thermal radiation, and it can be observed that as *Me* grows, the temperature distribution reduces while the thickness of the associated thermal boundary layer increases. Physically, raising the value of Me increases molecular mobility, which promotes energy dissipation and a decrease in fluid temperature. While the thermal condition of the liquid and its temperature boundary sheet significantly increase as the thermal radiation parameter increases when it is far from the wall in Figure 7, there is an increase in temperature profile near the wall because the radiation term describes the heat conduction contribution related to the heat radiation dispersion. Figure 8 depicts the thermophoresis term's and the angled magnetic field's influence on temperature profiles. Due to the conducting strength of nanoparticles, heat dispersion increases away from the stretched surface but diminishes when near to the wall. Furthermore, the temperature profile changes as the intensity of the magnetic field rises. Figure 9 depicts the consequences of β *and* α on mass species transfer patterns. The viscidity of the mass boundary layers decreases as the values of β *and* α enhance. Figure 10 depicts the effect of the Eckert number and the homogeneous reaction parameter K on concentration profiles. As the Eckert number increases, the mass species transfer distribution decreases, and the concentration decreases because reactants are burned during the homogeneous reaction, as shown in this figure. Figure 11 depicted the fluctuation in concentration profiles, and it was discovered that higher Ks values decay the concentration film. Physically, this is correct because as the reaction rate increases, the diffusion rate decreases, resulting in a decrease in species concentration. Figure 12 depicts the impact on concentration nanofilms of various generalized Schmidt number Sc and velocity ratio values. The concentration profile appears to increase as Sc values increase. The momentum diffusivity/mass diffusivity ratio is referred to as the Schmidt number. As a result, higher Schmidt values indicate lesser mass diffusivity.

Table 1: Comparison of numerical data $\left(-\theta'(0) \text{and} -\phi'(0)\right)$ for varying values of Nb and Nt when $\Pr = 10, \beta \to \infty, M = Me = N_R = T_R = E_c = A = K = S_c = K_s = 0$

		Khan and Pop [27]		Anwar et al. [28]		Present result	
Nb	**Nt**	$-\theta'(0)$	$-\phi'(0)$	$-\theta'(0)$	$-\phi'(0)$	$-\theta'(0)$	$-\phi'(0)$
0.1	0.1	0.9524	2.1294	0.9524	2.1294	0.9564398545488088	2.12393158517283
0.2	0.2	0.3654	2.5152	0.3654	2.5152	0.3690231431486497	2.5191630305413595
0.3	0.3	0.1355	2.6088	0.1355	2.6088	0.1348965693590891	2.6025084164995587
0.4	0.4	0.0495	2.6038	0.0495	2.6038	0.04942968955349425	2.6059193834130223
0.5	0.5	0.0179	2.5731	0.0179	2.5731	0.01733508188089205	2.5605058166716965

Table 2: Calculated results for the coefficient of wall-friction, Nusselt and concentration gradient numbers for diverse values of β, M P_r N_t N_R Me ks E_c K

β	M	P_r	N_t	N_R	Me	Ks	E_c	K	$\left(1+\frac{1}{\beta}\right)f''$	$-\left(1+Rt((TR-1)\theta+1)^3\right)$	g'
0.5	1.0	1.0	0.1	0.1	1.0	0.3	0.2	0.1	-0.723585	-0.22263	-0.20732
1.0									-0.883858	-0.191746	-0.207037
2.0									-1.01885	-0.171612	-0.206204
	0.0								-0.87913	-0.078617	-0.21943
	1.0								-1.13773	-0.157023	-0.205143
	2.0								-1.3465	-0.217058	-0.189454
		0.5							-1.1344	-0.08277	-0.174292
		0.6							-1.13521	-0.0980829	-0.174529
		0.7							-1.13595	-0.113094	-0.174746
			0.1						-1.13787	-0.15665	-0.175303
			0.3						-1.14615	-0.135553	-0.177655
			0.5						-1.15251	-0.119459	-0.179405
				0.2					-1.13248	-0.170477	-0.203444
				0.5					-1.14222	-0.145546	-0.206558
				0.8					-1.15253	-0.119411	-0.209664
					1.0				-1.13773	-0.157023	-0.205143
					2.0				-1.08247	-0.151087	-0.184176
					3.0				-1.03388	-0.145565	-0.158579
						0.1			-1.14248	-0.144893	-0.0870836
						0.2			-1.14234	-0.145258	-0.153894
						0.3			-1.14222	-0.145546	-0.206558
							0.2		-1.13773	-0.157023	-0.205143
							0.4		-1.08219	-0.302925	-0.184051
							0.6		-1.03312	-0.438861	-0.158111
								0.2	-1.13773	-0.157017	-0.202947
								0.4	-1.13774	-0.157	-0.197736
								0.6	-1.13775	-0.156973	-0.190922

5.0 CONCLUSION

This article presents the hydromagnetic flow of the melting surface for the Casson nanofluid past a stretchable surface with homogeneous and heterogeneous chemical reactions. The solutions were numerically obtained by the spectral collocation scheme. The influence of diverse fluid terms on the fluid motion, heat diffusion and nanoparticle mass fields were discussed and presented graphically. Also, the effect of bodily terms on the skin friction, temperature gradient and mass gradient numbers were analyzed and obtainable in the table 1. Below are the summary of our numerical results.

- Enhancement of temperature field is observed when temperature ratio, thermal radiation, magnetic field, Eckert number, and Casson parameter is increased.
- Concentration profiles diminish for a higher number of melting parameters, homogeneous and heterogeneous reactions.
- Flow rate motion field is damped for larger magnetic term values and Casson parameter
- The temperature boundary film tends to drop with augmented Prandtl number and melting parameter.
- The concentration distribution was enhanced and associated concentration boundary layer thickness was decreased for increasing values of the Schmidt number.

REFERENCES

[1] Ahmad, K., Wahid, Z., and Hanouf, Z. “Heat transfer analysis for Casson fluid flow over a stretching sheet with Newtonian heating and viscous dissipation”, IOP Conf. Series: *Journal of Physics*: Conf. Series 1127 (2019) 012028 IOP Publishing doi:10.1088/1742-6596/1127/1/012028.

[2] Anwar, M. I., Rafique, K., Misiran, M., and Shehzad, S. A. “Numerical study of the hydrodynamic flow of a Casson nanomaterial past an inclined sheet under porous medium”, *Heat Transfer*—Asian Res. (2019) 1–28.

[3] Kumar, P. S., and Gangadhar, K. “Effect of chemical reaction on slip flow of MHD Casson fluid over a stretching sheet with heat and mass

transfer", *Advances in Applied Science Research*, 2015, 6(8):205-223.

[4] Mahanthesh, B., and Gireesha, B. J., "Thermal Marangoni convection in two-phase flow of dusty Casson fluid", Results in Physics 8 (2018) 537–544.

[5] Vijayaragavan, R., and Karthikeyan, S. "Hall Current Effect on Chemically Reacting MHD Casson Fluid Flow with Dufour Effect and Thermal Radiation", *Asian Journal of Applied Science and Technology* (AJAST), Volume 2, Issue 2, Pages 228-245, 2018.

[6] Ramadevi, B., Ramana Reddy, J. V., and Sugunamma, V. "Influence of thermodiffusion on Time-dependent Casson fluid flow past a wavy surface", *International Journal of Mathematical, Engineering and Management Sciences* (2018) ISSN: 2455-7749.

[7] Akaje, T. W., and Olajuwon, B. I. "Effects of inclined magnetic field and slip boundary condition on heat and mass transfer in a Casson nanofluid flow over a stretching sheet", *Sciences & Technology* Vol 5-N1, June 2020, pp. 15-28.

[8] Hamid, M., Usman, M., Khan, Z.H., Ahmad, R., and Wang, W. "Dual solutions and stability analysis of flow and heat transfer of Casson fluid over a stretching sheet", *Phys. Lett*. A, 383(20), 2400-2408, 2019.

[9] Jabeen, K., Mushtaq, M., and Muntazir, R. M. A. "Analysis of MHD fluids around a linearly stretching sheet in porous media with thermophoresis, radiation, and chemical reaction", *Mathematical Problems in Engineering*. 14pg, vol. 2020, Article ID 9685482.

[10] Lund, L.A., Omar, Z., Khan, I., Baleanu, D., and Nisar, K.S. "Dual similarity solutions of MHD stagnation point flow of Casson fluid with the effect of thermal radiation and viscous dissipation: stability analysis", *Scientific Reports*. 10:15405, 2020.

[11] Kumar, K. G., Gireesha, B. J., Rudraswamy, N. G. and Gorla, R. S. R. "Melting heat transfer of hyperbolic tangent fluid over a stretching sheet with fluid-particle suspension and thermal radiation", *Communications in Numerical Analysis*, No. 2, 125-140, 2017.

[12] Khan, W. A., Khan, M., Irfan, M., and Alshomrani, A. S. "Impact of melting heat transfer and nonlinear radiative heat flux mechanisms for the generalized Burgers fluids", *Results in Physics 7*, 4025–4032, 2017.

[13] Mabood, F., and Das, K. "Outlining the impact of melting on MHD Casson fluid flow past a stretching sheet in a porous medium with radiation", *Heliyon 5* (2019) e01216.DOI: 10.1016/j.heliyon.2019.e01216

[14] Sarkar, S and Endalew, M. F. "Effects of melting process on the hydromagnetic wedge flow of a Casson nanofluid in a porous medium", *Boundary Value Problems*, 1-14, 2019, https://doi.org/10.1186/s13661-019-1157-5.

[15] Korawan, A. D., Soeparman, S., Wijayanti, W., and Widhiyanuriyawan, D. "Increased melting heat transfer in the latent heat energy storage from the tube-and-shell model to the combine-and-shell model", *Modelling and Simulation in Engineering* Volume, Article ID 8574184, 9 pages, 2017, https://doi.org/10.1155/2017/8574184.

[16] Merkin, J. H. "A model for isothermal homogeneous-heterogeneous reactions in Boundary-Layer flow", *Math Comput Modell* 1996;24:125–36.

[17] Khan, N., Hashmi, M. S., Khan, S. U., Chaudhry, F., Iskander, T., and Mostafa, S. S. "Effects of homogeneous and heterogeneous chemical features on Oldroyd-B fluid flow between stretching disks with velocity and temperature boundary assumptions", *Mathematical Problems in Engineering*, Volume 2020, Article ID 5284906, 13 pages.

[18] Khan, I., Malik, M. Y., Hussain, A., Salahuddin, T. "Effect of homogenous-heterogeneous reactions on MHD Prandtl fluid flow over a stretching sheet", *Results in Physics 7* (2017) 4226–4231.

[19] Malik, R. A., and Khan, M. "Numerical study of homogeneous–heterogeneous reactions in Sisko fluid flow past a stretching cylinder", *Results in Physics 8* (2018) 64–70.

[20] Suleman, M., Ramzan, M., Ahmad, S., and Lu, D. "Numerical simulation for homogeneous–heterogeneous reactions and Newtonian heating in the silver-water nanofluid flow past a nonlinear stretched cylinder", *Phys. Scr*. 94 (2019) 085702 (9pp).

[21] Sheikh, M., and Abbas, Z. "Homogeneous–heterogeneous reactions in stagnation point flow of Casson fluid due to a stretching/shrinking sheet with uniform suction and slip effects", *Ain Shams Engineering Journal* (2017) 8, 467–474.

[22] Ahmed, S., Xu, H., and Sun, Q. "Stagnation Flow of an SWCNT Nanofluid towards a Plane Surface with Heterogeneous-Homogeneous Reactions", *Mathematical Problems in Engineering*, Volume 2020, Article ID 3265143, 12 pages, https://doi.org/10.1155/2020/3265143.

[23] Yahaya, R. I., Md Arifin, N., and Mohamed Isa, S. S. P. "Stability Analysis on Magneto-hydrodynamic Flow of Casson Fluid over a Shrinking Sheet with Homogeneous-Heterogeneous Reactions", *Entropy 2018*, 20, 652; doi:10.3390/e20090652.

[24] Bachok, N., Ishak, A., and Pop, I. "On the stagnation-point flow towards a stretching sheet with homogeneous–heterogeneous reactions effects", *Commun Nonlinear Sci Numer Simulat* 2011;16(11):4296–302.

[25] Hayat, T., Imtiaz, M., and Alsaedi, A. "Impact of magnetohydrodynamics in the bidirectional flow of nanofluid subject to second-order slip velocity and homogeneous–heterogeneous reactions", *J. Magn. Magn. Mater*. 2015; 395 (1):294–302.

[26] Ehrenstein, U., and Peyret, R. A. "Chebyshev spectral collocation method for the Navier-Stokes equations with application to double-diffusive convection", *Int J Number Meth Fl*. 1989;9:427–452.

[27] Khan, W., and Pop, I. "Boundary-layer flow of a nanofluid past a stretching sheet", *Int. J Heat Mass Transfer*. 2010;53:2477-2483

[28] Anwar, M. I., Rafique, K., Misiran, M., and Shehzad, S. A. "Numerical study of the hydrodynamic flow of a Casson nanomaterial past an inclined sheet under porous medium", *Heat Transfer-Asian Res*. 2019;1–28. https://doi.org/10.1002/htj.21614